



1 **Multiphase Reaction of SO₂ with NO₂ on CaCO₃ Particles. 1.**

2 **Oxidation of SO₂ by NO₂**

3 Defeng Zhao[‡], Xiaojuan Song[‡], Tong Zhu*, Zefeng Zhang, Yingjun Liu

4 SKL-ESPC and BIC-ESAT, College of Environmental Sciences and Engineering, Peking University, Beijing, 100871, China

5 [‡]These authors contributed equally to this work.

6 *Correspondence to: Tong Zhu (tzhu@pku.edu.cn)

7 **Abstract.** Heterogeneous/multiphase reaction of SO₂ with NO₂ on solid or aqueous particles is thought to be a
8 potentially important source of sulfate in the atmosphere, for example, during heavily polluted episodes (haze),
9 but the reaction mechanism and rate are uncertain. In this study, we investigated the heterogeneous/multiphase
10 reaction of SO₂ with NO₂ on individual CaCO₃ particles in N₂ using Micro-Raman spectroscopy in order to
11 assess the importance of the direct oxidation of SO₂ by NO₂. In the SO₂/NO₂/H₂O/N₂ gas mixture, the CaCO₃
12 solid particle was first converted to the Ca(NO₃)₂ droplet by the reaction with NO₂ and the deliquescence of
13 Ca(NO₃)₂, and then NO₂ oxidized SO₂ in the Ca(NO₃)₂ droplet forming CaSO₄, which appeared as needle-shaped
14 crystals. Sulfate was mainly formed after the complete conversion of CaCO₃ to Ca(NO₃)₂, that is, during the
15 multiphase oxidation of SO₂ by NO₂. The precipitation of CaSO₄ from the droplet solution promoted sulfate
16 formation. The reactive uptake coefficient of SO₂ for sulfate formation is on the order of 10⁻⁸, and RH enhanced
17 the uptake coefficient. We estimate that the direct multiphase oxidation of SO₂ by NO₂ is not an important source
18 of sulfate in the ambient atmosphere compared with the SO₂ oxidation by OH in the gas phase.



19 1 Introduction

20 Sulfate is a major component of atmospheric particulate matter. It contributes to a large fraction of
21 atmospheric aerosol particles in both urban and rural areas (Seinfeld and Pandis, 2006; Zhang et al., 2007).
22 Sulfate is either from primary source, such as sea spray, or from secondary source, i.e., by the oxidation of
23 reduced sulfur compounds such as dimethyl sulfide (DMS), carbonyl sulfur (COS), and SO₂ (Seinfeld and Pandis,
24 2006). In the continent, the main source of sulfate is the oxidation of SO₂, an important air pollutant from fossil
25 fuel combustion. SO₂ can be oxidized in the gas phase, mainly by OH, or in the particle phase such as by H₂O₂,
26 O₃, or O₂ catalyzed by transition metal ions in cloud or fog water (Seinfeld and Pandis, 2006; Finlayson-Pitts and
27 Pitts Jr., 1999) or by O₃ or photochemical reactions on particle surface (Zhu et al., 2011; Li et al., 2006; Li et al.,
28 2007; Shang et al., 2010; Li et al., 2011).

29 Although various pathways of SO₂ oxidation are identified, the source of sulfate and relative importance of
30 various pathways of SO₂ oxidation forming sulfate in the atmosphere still remain uncertain. For example, during
31 heavily polluted episodes (haze) in China in recent years, high concentrations of sulfate were observed, but the
32 source of sulfate is elusive (Wang et al., 2016; Wang et al., 2014a; Zheng et al., 2015b; Guo et al., 2014). The
33 relative contribution of regional transport versus local formation and physical and chemical mechanisms
34 responsible for sulfate formation are still not clear. Recent studies have highlighted heterogeneous reactions of
35 SO₂ on solid or liquid particles to be a possibly important source of sulfate based on model, field and laboratory
36 studies (Huang et al., 2014; Zhu et al., 2011; Cheng et al., 2016; Gao et al., 2016; Zheng et al., 2015a; Wang et al.,
37 2014b; He et al., 2014; Fu et al., 2016; Xue et al., 2016; Xie et al., 2015). During haze episodes, relative humidity
38 (RH) is often high (Zhang et al., 2014; Wang et al., 2016; Zheng et al., 2015b) and particles or some components
39 of particles can deliquesce forming liquid water. In particular, several recent studies propose that the multiphase
40 oxidation of SO₂ by NO₂, another important air pollutant, on liquid particles may be a major pathway of sulfate
41 formation (Cheng et al., 2016; Wang et al., 2016; Xue et al., 2016; Xie et al., 2015). Both SO₂ and NO₂ are from
42 fossil fuel combustion and both concentrations are often high during haze episodes, and their reaction may
43 significantly contribute to sulfate formation.

44 In order to assess and quantify the role of the heterogeneous reactions of SO₂ in sulfate formation, laboratory
45 studies are needed to understand the reaction process and obtain kinetic parameters for modeling such as uptake
46 coefficients of SO₂. Among many studies investigating the heterogeneous reactions of SO₂ on various particles
47 (Goodman et al., 2001; Li et al., 2011; Shang et al., 2010; Huang et al., 2015; Huang et al., 2016; Zhou et al.,
48 2014; Li et al., 2004; Kong et al., 2014; Passananti et al., 2016; Cui et al., 2008; Chu et al., 2016; Zhao et al.,
49 2015; Li et al., 2006; Wu et al., 2011; He et al., 2014; Liu et al., 2012; Ma et al., 2008; Park and Jang, 2016;
50 Ullerstam et al., 2002; Sorimachi et al., 2001; Ullerstam et al., 2003; Wu et al., 2013; Wu et al., 2015), only a few
51 have investigated the heterogeneous reaction of SO₂ in the presence of NO₂ (He et al., 2014; Liu et al., 2012; Ma
52 et al., 2008; Park and Jang, 2016; Ullerstam et al., 2003; Ma et al., 2017). These studies found that NO₂ can
53 promote sulfate formation from SO₂ oxidation (He et al., 2014; Liu et al., 2012; Ma et al., 2008; Park and Jang,
54 2016; Ullerstam et al., 2003). However, the mechanism of this effect is still not clear and only few studies
55 reported kinetic parameters such as uptake coefficient of SO₂ in the presence of NO₂. Importantly, most of these
56 studies focused on the gas-solid reactions on particles. Very few laboratory studies have investigated the
57 multiphase reaction of SO₂ with NO₂ on atmospheric aqueous particles or solid-aqueous mixed phase aerosol



58 particles, and the uptake coefficient of SO₂ on atmospheric aqueous particles due to the reaction with NO₂ is
59 largely unknown. From several decades ago until now, a number of studies have investigated the aqueous
60 reaction of soluble S(IV) species (H₂SO₃, HSO₃⁻, SO₃²⁻) with NO₂ in dilute bulk solution (Lee and Schwartz,
61 1983; Ellison and Eckert, 1984; Clifton et al., 1988; Littlejohn et al., 1993) relevant to the conditions in cloud
62 water. However, in aqueous aerosol particles, the reaction rate and process may be substantially different from in
63 bulk solution due to high ion strength resulted from high concentrations of solutes, potential interactions of
64 sulfate with other ions, and low water activity in aerosol particles.

65 In this study, we investigated the heterogeneous reaction of SO₂ with NO₂ on CaCO₃ particles at the ambient
66 RH. CaCO₃ is an important component of mineral aerosols, especially in East Asia (Cao et al., 2005; Song et al.,
67 2005; Okada et al., 2005) and it is a very reactive component (Krueger et al., 2004; Li et al., 2010; Li et al., 2006;
68 Prince et al., 2007a). It is also one of the few alkaline particles in the atmosphere, especially in northern China,
69 which can neutralize acids on particles and increase the pH of aerosol water, thus promoting the apparent
70 solubility and uptake of SO₂. The reaction of SO₂ with NO₂ on CaCO₃ has been suggested by field observations,
71 which showed internal mixing of CaCO₃, CaSO₄, and Ca(NO₃)₂ in particles (Hwang and Ro, 2006; Li and Shao,
72 2009; Zhang et al., 2000). More importantly, as shown below, during the reaction on CaCO₃, aqueous phase can
73 be formed, which allows us to investigate the multiphase reaction of SO₂ with NO₂. We studied the reaction of
74 SO₂ and NO₂ on individual CaCO₃ particles using Micro-Raman spectrometer with a flow reaction system.
75 Combining the chemical and optical information from Micro-Raman spectrometer, we systematically
76 investigated the reaction process and quantified the reactive uptake coefficient of SO₂ due to the oxidation by
77 NO₂ based on sulfate production rate. We further assessed the importance of the multiphase reaction of SO₂ with
78 NO₂ in the atmosphere. In this study, we present the findings of this reaction in N₂. We used N₂ instead of air as a
79 carrier gas to exclude the inference of O₂ in SO₂ oxidation, which is key to elucidate the direct oxidation of SO₂
80 by NO₂. In a companion paper we shall report the findings of the multiphase reaction of SO₂ with NO₂ in air to
81 explore the role of O₂ in this reaction.

82 2 Experimental

83 2.1 Apparatus and procedures

84 The experimental setup used in this study is illustrated in Fig. 1. The details of the setup have been described
85 previously (Liu et al., 2008; Zhao et al., 2011). NO₂ and SO₂ of certain concentrations were prepared by adjusting
86 the flow rates of standard gases of specified concentrations (NO₂: 1000 ppm in N₂, Messer, Germany; SO₂: 2000
87 ppm in N₂, National Institute of Metrology P.R.China) and high-purity nitrogen (99.999%, Beijing
88 Haikeyuanchang Corp.). RH was regulated by adjusting the flow rates of humidified N₂ and of dry N₂ and other
89 dry gases. Humidified N₂ was prepared by bubbling N₂ through fritted glass in water. Flow rates of the gases
90 were controlled by mass flow controllers (FC-260, Tylan, Germany). Mixed gases reacted with CaCO₃ particles
91 in a stainless steel reaction cell. Individual CaCO₃ particles were deposited on a Teflon FEP film substrate
92 annealed to a silicon wafer. The substrate was then placed in the reaction cell, which has a glass cover on top of
93 the center. Through this top window, a Micro-Raman spectrometer (LabRam HR800, HORIBA Jobin Yvon) was
94 used to acquire the Raman spectra of particles. A 514 nm excitation laser was focused onto selected particles and



95 back scattering Raman signals were detected. The details of the instrument are described in previous studies (Liu
96 et al., 2008; Zhao et al., 2011).

97 The RH and temperature of the outflow gas from the reaction cell were measured by a hygrometer (HMT100,
98 Vaisala). Experiments of individual CaCO_3 particles reacting with NO_2 (75-200 ppm) and SO_2 (75-200 ppm)
99 mixing gas diluted with N_2 were conducted under certain RH (17-72%). All the measurements were carried out at
100 25 ± 0.5 °C. Each reaction was repeated for three times.

101 In this study, the size of CaCO_3 particles was around 7-10 μm . During a reaction, components of an
102 individual particle may distribute unevenly within the particle due to the formation of new aqueous phase or solid
103 phase, and particles may grow. Because particles are larger than the laser spot (~ 1.5 μm), Raman spectrum from
104 one point does not represent the chemical composition of the whole particle. Therefore Raman mapping was used
105 to obtain the spectra on different points of a particle in order to get the chemical information of the whole particle.
106 The mapping area is a rectangular slightly larger than the particle and mapping steps are 1×1 μm . Raman spectra
107 in the range 800-3900 cm^{-1} were acquired with exposure time of 1 s for each mapping point. During each
108 mapping (7-10 min, depending on the mapping area), no noticeable change in composition was detected. The
109 mean time of a mapping period was used as reaction time. During the reaction, microscopic images of particles
110 were also recorded. Raman spectra were analyzed using Labspec 5 software (HORIBA Jobin Yvon). Raman
111 peaks were fit to Gaussian-Lorentzian functions to obtain peak positions and peak areas on different points of the
112 particle. The peak areas were then added up to get the peak area for the whole particle.

113 Besides the reaction of CaCO_3 with SO_2 and NO_2 , other reaction systems including the reaction on $\text{Ca}(\text{NO}_3)_2$,
114 NaNO_3 , NH_4NO_3 particles with SO_2 or SO_2 and NO_2 mixing gas (summarized in Table 1) were also studied in
115 order to elucidate the reaction mechanism.

116 CaCO_3 (98%, Sigma) with diameters about 7-10 μm on average, $\text{Ca}(\text{NO}_3)_2 \cdot 4\text{H}_2\text{O}$ (ACS, 99-103%; Riedel-de
117 Haën), NH_4NO_3 (AR, Beijing Chemical Works), and NaNO_3 (AR, Beijing Chemical Works) were used without
118 further purification.

119 2.2 Quantification of reaction products on the particle phase

120 The Raman intensity of a sample is described as Equation (1):

$$121 I(\nu) = I_0 \cdot A(\nu) \cdot J(\nu) \cdot \nu^4 \cdot D \cdot K \quad (1)$$

122 where I_0 is the intensity of incident laser, $A(\nu)$ is the collection efficiency function of Raman spectrometer,
123 $J(\nu) \cdot \nu^4$ is the Raman scattering section of the sample, D is the number density of the sample, and K is the
124 effective depth of the sample. Raman intensity is not only determined by the amount of the sample molecules, but
125 also by the configuration of the instrument, whose influence cannot be eliminated unless internal standards are
126 used. For soluble compounds, water can be used an internal standard (Zhao et al., 2011; Liu et al., 2008).
127 However, in this study, one product (CaSO_4 , see below) appeared as solid state. For solid particles of micro-scale,
128 it is hard to add internal standards into the system. Therefore it is difficult to establish the relationship between
129 Raman intensity and the amount of sample molecules, which makes the quantification very challenging.

130 In this study, we chose seven individual CaSO_4 particles varying in size as the standard for solid products.
131 The profile of each particle can be obtained by scanning the particle using Raman mapping with steps of 1, 1, and
132 2 μm for x, y, and z dimension, respectively. The volume of each particle was calculated based on 3D profiles of



133 the particles using a CAD software (AutoDesk). In order to minimize the influence variations of incident laser on
134 Raman intensity. These seven particles were measured before each experiment, which produced a calibration
135 curve for each experiment (Fig. S1).

136 2.3 Determination of reactive uptake coefficient

137 In this study, sulfate was produced from the oxidation of SO₂. The reactive uptake coefficient γ of SO₂ on
138 individual particles was estimated from sulfate formation. γ is derived as the rate of sulfate formation
139 ($d\{\text{SO}_4^{2-}\}/dt$) divided by the rate of surface collisions with an individual particle (Z),

$$140 \gamma = \frac{d\{\text{SO}_4^{2-}\}}{Z dt} . \quad (2)$$

$$141 Z = \frac{1}{4}cA_s[\text{SO}_2], \quad (3)$$

$$142 c = \sqrt{\frac{8RT}{\pi M_{\text{SO}_2}}} , \quad (4)$$

143 where R is the gas constant, T is temperature, M_{SO_2} is the molecular weight of SO₂, and c is the mean
144 molecular velocity of SO₂, A_s is the surface area of an individual particle. Z is the collision rate between SO₂ and
145 a particle. $\{\text{SO}_4^{2-}\}$ indicates the amount of sulfate on the particle phase in mole, and $[\text{SO}_2]$ indicates the
146 concentration of SO₂ in the gas phase.

147 $\{\text{SO}_4^{2-}\}$ was determined by a calibration curve as stated above. In this study, since sulfate was mainly
148 formed after the formation of Ca(NO₃)₂ droplet as shown below, A_s was calculated by estimating the diameter of
149 the droplet according to its microscopic image and using a shape of spherical segment defined by the contact
150 angle water droplet on Teflon (Good and Koo, 1979). For each experiment, at least three particles with different
151 diameters were measured to get an average reactive uptake coefficient.

152 3 Results and discussion

153 3.1 Reaction products and particle morphology changes

154 Figure 2 shows typical Raman spectra of a CaCO₃ particle during the reaction with SO₂ and NO₂. The peak
155 at 1087 cm⁻¹ is assigned to the symmetric stretching mode of carbonate (ν_1) (Nakamoto, 1997), which could be
156 detected during the initial stage of the reaction. Shortly after the reaction started, a peak at 1050 cm⁻¹ was
157 observed, which is attributed to the symmetric stretching mode of nitrate (ν_1). This demonstrates that calcium
158 nitrate (Ca(NO₃)₂) was produced during the reaction. A broad band at 2800-3800 cm⁻¹ was also observed together
159 with the formation of Ca(NO₃)₂. It is assigned to -OH stretching of liquid water. The formation of liquid water is
160 attributed to the deliquescence of Ca(NO₃)₂, which is very hygroscopic and can deliquesce at ~10% RH (Liu et al.,
161 2008; Al-Abadleh et al., 2003; Tang and Fung, 1997). After about 82 min, a new peak at 1013 cm⁻¹ was observed,
162 which is attributed to the symmetric stretching mode of sulfate (ν_1) in anhydrite (CaSO₄) (Sarma et al., 1998).
163 This peak clearly demonstrates that sulfate was formed. CaSO₄ as a reaction product has also been found in the
164 reaction of CaCO₃ with SO₂ and NO₂ in a previous study (Ma et al., 2013b). Afterwards, no other Raman peaks
165 than those of CaCO₃, Ca(NO₃)₂, and CaSO₄ were detected until 1050 min after the reaction.



166 Concomitant with the formation of $\text{Ca}(\text{NO}_3)_2$ and CaSO_4 , the microscopic morphology of the particle
167 changed significantly. The initial CaCO_3 particle was a crystal close to a rhombohedron of about 9-10 μm (Fig.
168 3a). After reacting with NO_2/SO_2 , the surface of the particle became smoother, and then a liquid layer formed
169 surrounding the solid particle core (Fig. 3c). Raman spectra of the particle reveal that the outer liquid layer
170 consisted of $\text{Ca}(\text{NO}_3)_2$ and water. As the reaction proceeded, the solid CaCO_3 core diminished gradually and
171 finally CaCO_3 was completely consumed and a $\text{Ca}(\text{NO}_3)_2$ spherical droplet was formed (Fig. 3d). The whole
172 particle became larger due to the growth of the outer liquid layer. The diameter of the $\text{Ca}(\text{NO}_3)_2$ droplet reached
173 $\sim 16 \mu\text{m}$, and the droplet did not change much in the subsequent period of the reaction. Despite the invariant
174 droplet diameter, a new solid phase of needle-shaped crystals was formed as the reaction proceeded, which
175 distributed unevenly in the droplet. The Raman spectra of the new solid phase and Raman mapping (Fig. S2)
176 reveal that this solid matter was CaSO_4 . The amount of CaSO_4 increased gradually during the reaction, and its
177 Raman peak could be observed more clearly at 1050 min.

178 3.2 Reaction process

179 In order to learn about the reaction process and mechanism, the amounts of $\text{Ca}(\text{NO}_3)_2$, CaSO_4 , and CaCO_3 ,
180 represented by the peak area at 1050, 1013, and 1087 cm^{-1} in Raman spectra, respectively, were investigated as a
181 function of reaction time. As shown in Fig. 4, $\text{Ca}(\text{NO}_3)_2$ was produced before CaSO_4 . Nitrate was detected
182 immediately after the reaction started, and reached a maximum at ~ 50 min whereas sulfate did not reach the
183 detection limit until 82 min of the reaction. Sulfate increased slowly in the reaction and we did not observe it
184 leveling off even after 1050 min.

185 According to the time series of carbonate, nitrate, and sulfate, this reaction consisted of two successive
186 processes. The first process was the formation of $\text{Ca}(\text{NO}_3)_2$, which was accompanied with the consumption of
187 CaCO_3 (Fig. 4), indicating that $\text{Ca}(\text{NO}_3)_2$ was produced due to the reaction of CaCO_3 with NO_2 . The detailed
188 mechanism of the formation of $\text{Ca}(\text{NO}_3)_2$ in the reaction CaCO_3 with NO_2 have been studied by Li et al. (2010).
189 The second process was the formation of CaSO_4 through the oxidation of SO_2 . CaSO_4 was mainly produced after
190 CaCO_3 was completely consumed and increased steadily as the reaction proceeded.

191 3.3 Reaction mechanism

192 3.3.1 Mechanism of sulfate formation

193 Based on the results above, we found that a series of reactions of SO_2 and NO_2 on a CaCO_3 particle led to
194 sulfate formation. Almost the entire sulfate was produced after a CaCO_3 particle was converted to a $\text{Ca}(\text{NO}_3)_2$
195 droplet (Fig. 4), although in some experiments a trace amount of sulfate could be observed when a small amount
196 of CaCO_3 was still left in the $\text{Ca}(\text{NO}_3)_2$ droplet. The absence or low amount of sulfate before CaCO_3 was
197 completely consumed might be due to the competition between the reaction of aqueous NO_2 with CaCO_3 and the
198 reaction with SO_2 . This result suggests that forming a $\text{Ca}(\text{NO}_3)_2$ droplet was key to the formation of sulfate.

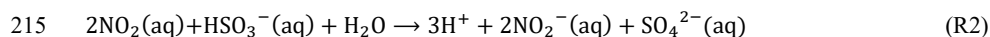
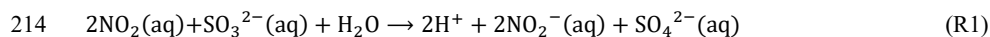
199 This finding is further supported by the results of the reaction of SO_2 with NO_2 on a $\text{Ca}(\text{NO}_3)_2$ droplet (Fig. 5
200 and Table 1). Using a $\text{Ca}(\text{NO}_3)_2$ droplet as the reactant, the reaction with SO_2/NO_2 at the same condition still
201 produced CaSO_4 , confirming CaCO_3 was not necessary for sulfate formation. The reaction with $\text{Ca}(\text{NO}_3)_2$



202 produced similar amount of sulfate to the reaction with CaCO_3 based on Raman spectra and microscopic images
 203 (Fig. 5), which indicates that $\text{Ca}(\text{NO}_3)_2$ droplet was important for sulfate formation. Therefore, we conclude that
 204 SO_2 was mainly oxidized via the multiphase reaction on the $\text{Ca}(\text{NO}_3)_2$ droplet while CaCO_3 mainly worked as a
 205 precursor of the $\text{Ca}(\text{NO}_3)_2$ droplet.

206 The oxidant of SO_2 can be NO_3^- or NO_2 in the $\text{Ca}(\text{NO}_3)_2$ droplet here. In a reaction between $\text{Ca}(\text{NO}_3)_2$
 207 droplets and SO_2 (150 ppm) under 72% RH, we did not observe any sulfate formation on the basis of the Raman
 208 spectra and microscopic image after 5 h of reaction. This indicates that NO_3^- was not the oxidant for SO_2 in our
 209 study, which was also consistent with a previous study (Martin et al., 1981). Therefore, we conclude that SO_2 was
 210 oxidized by NO_2 in the $\text{Ca}(\text{NO}_3)_2$ droplet.

211 According to previous studies, NO_2 can oxidize sulfite and bisulfite ions into sulfate ion in aqueous phase
 212 (Ellison and Eckert, 1984; Shen and Rochelle, 1998; Littlejohn et al., 1993). The overall mechanism was
 213 described to be (Clifton et al., 1988):



216 Under the experimental conditions of our study, water uptake of $\text{Ca}(\text{NO}_3)_2$ led to condensation of liquid
 217 water, which provided a site for aqueous oxidation of S(IV) by NO_2 . The relative fractions of the three S(IV)
 218 species depend on pH and the equilibrium between them is fast (Seinfeld and Pandis, 2006). The pH of the
 219 droplet was mainly determined by the gas-aqueous equilibrium of SO_2 in this study and estimated to be ~ 3 and
 220 thus main S(IV) species was HSO_3^- . Then SO_4^{2-} from S(IV) oxidation can react with Ca^{2+} forming CaSO_4
 221 precipitation as observed in Raman spectra due to the low value of K_{sp} for CaSO_4 (Lide, 2009):



223 Some previous studies have shown that SO_2 can react with CaCO_3 to produce calcium sulfite (CaSO_3) (Li et
 224 al., 2006; Prince et al., 2007b; Ma et al., 2013a), and CaSO_3 can be oxidized to CaSO_4 by NO_2 (Rosenberg and
 225 Grotta, 1980; Ma et al., 2013a). In our study, we investigated the reaction between CaCO_3 and SO_2 (150 ppm) at
 226 72% RH. We found that both sulfate and sulfite were lower than the detection limit of our Raman spectrometer
 227 even after 300 min of the reaction. This indicates that forming CaSO_3 was not the main pathway in CaSO_4
 228 formation in our study and CaCO_3 did not directly contribute to the formation of CaSO_4 .

229 3.3.2 Effects of cations in sulfate formation

230 Since sulfate was observed to precipitate as CaSO_4 , we further analyzed the effect of precipitation reaction
 231 and cations on the aqueous oxidation of SO_2 by NO_2 . The spontaneity of the SO_2 oxidation by NO_2 for Reaction
 232 (R2) can be analyzed using the reaction Gibbs energy as follows:

$$233 \quad \Delta_r G = \Delta_r G^\theta + RT \ln \frac{a_{\text{H}^+}^3 \cdot a_{\text{SO}_4^{2-}} \cdot a_{\text{NO}_2}^2}{a_{\text{NO}_2(\text{aq})}^2 \cdot a_{\text{HSO}_3^-}} \quad (5)$$

234 where $\Delta_r G$ is the reaction Gibbs energy, $\Delta_r G^\theta$ is the standard reaction Gibbs energy, R is the gas constant, T
 235 is temperature, and a is the activity of various species.

236 The precipitation of CaSO_4 can substantially decrease the activity of SO_4^{2-} , and thus decrease $\Delta_r G$ and
 237 promote the oxidation of SO_2 and sulfate formation. In order to test effects of cations, we replaced Ca^{2+} with Na^+
 238 or NH_4^+ . Based on Raman spectra, we found that in the reaction of a NaNO_3 or a NH_4NO_3 droplet with NO_2/SO_2



239 no sulfate was formed after 300 min in the same reaction conditions as $\text{Ca}(\text{NO}_3)_2$ and CaCO_3 (Fig. 6 and Table 1).
240 Accordingly, no CaSO_4 solid particles were observed in these droplets. Therefore, we concluded that the
241 precipitation of less soluble CaSO_4 promoted the forward reaction, i.e., sulfate formation.

242 3.4 Reactive uptake coefficient of SO_2

243 The reactive uptake coefficients of SO_2 (γ) for sulfate formation under different conditions are shown in
244 Table 2. Each reaction was repeated for three times, during which, three particles with different size were
245 selected. γ was higher at higher relative humidity, suggesting again that liquid water plays an important role in
246 the formation of CaSO_4 . At 17% RH, the reaction between CaCO_3 and NO_2 (the first process of the whole
247 reaction) proceeded very slowly, and the amount of liquid water formed due to the water uptake of $\text{Ca}(\text{NO}_3)_2$ was
248 very low. As a result, we did not observe the formation of CaSO_4 (the second process of the whole reaction) after
249 1000 min of the reaction and even at higher SO_2 and NO_2 concentrations (200 ppm SO_2 , 200 ppm NO_2). Under
250 higher relative humidity (46% and 72% RH), sulfate was observed soon after the reaction. It is interesting to note
251 that there were no significant difference for γ between 46% and 72% RH. In either case, the reaction between
252 CaCO_3 and NO_2 proceeded quickly and CaCO_3 was completely converted to a $\text{Ca}(\text{NO}_3)_2$ droplet within 100 min
253 after the reaction. In the presence of enough liquid water, RH seemed to be no longer a limiting factor. In such
254 conditions, an increase of NO_2 concentration (from 75 ppm to 200 ppm at 72% RH) promoted the reactive uptake
255 of SO_2 .

256 The reactive uptake coefficient of SO_2 for sulfate formation was determined to be on the order of 10^{-8} at 46%
257 and 72% RH. This value is higher than the uptake coefficient (10^{-10}) on mineral particles sampled from Cape
258 Verde Islands (the main contents being potassium feldspars and quartz) obtained by Ullerstam et al. (2003) using
259 NO_2/SO_2 mixing gas and DRIFTS technique. But the uptake coefficient in this study is lower than the uptake
260 coefficient of SO_2 on ATD particles in the presence of NO_2 ($(2.10 \pm 0.08) \times 10^{-6}$) determined by Park and Jang
261 (2016). γ here is also much lower than the γ of SO_2 on oxalic acid particles in the presence of NO_2 and NH_3
262 ($10^{-6} \sim 10^{-4}$) determined at varying RH reported by Wang et al. (2016). The difference in these uptake coefficients
263 is attributed to the different chemical composition of particles, reaction mechanism, reaction conditions, and the
264 ways that the particle surface is determined. It is worth noting that in the studies of Ullerstam et al. (2003) and
265 Park and Jang (2016), particles exist as solid state and sulfate formation is via gas-solid heterogeneous reaction,
266 and in the study of Wang et al. (2016) sulfate formation is stated to be via aqueous reaction. In this study sulfate
267 formation was via gas-liquid-solid multiphase reaction and liquid water played a key role.

268 In the ambient atmosphere, the reactive uptake coefficient of SO_2 due to the multiphase oxidation by NO_2 is
269 influenced by various factors such as RH, NO_2 concentration, pH, sulfate concentration, and the presence of other
270 ions in aerosol particles. For example, NO_2 concentrations in the atmosphere are much lower than those used in
271 this study. At lower NO_2 concentrations, the uptake coefficient of SO_2 decreases, because the oxidation rate of
272 SO_2 in aqueous phase decreases with decreasing NO_2 concentration. In addition, aqueous sulfate concentrations
273 in aerosol particles in the atmosphere are often high, which may suppress the reaction of SO_2 with NO_2 according
274 to the discussion above and Equation (5), and thus reduce the uptake coefficient of SO_2 . Therefore, the reactive
275 uptake coefficient of SO_2 obtained in this study (10^{-8} at 46-72% RH and 75 ppm NO_2) can be regarded as an



276 upper limit of the reactive uptake coefficient of SO₂ due to the multiphase reaction with NO₂ in the ambient
277 atmosphere.

278 4 Conclusion and implications

279 We investigated the heterogeneous reaction of SO₂ with NO₂ on individual CaCO₃ particles in N₂ using
280 Micro-Raman spectrometry. The reaction first converted the CaCO₃ particle to the Ca(NO₃)₂ droplet via the
281 reaction with NO₂ in the SO₂/NO₂/H₂O/N₂ gas mixture and the deliquescence of Ca(NO₃)₂, and then formed
282 needle-shaped CaSO₄ crystals in the Ca(NO₃)₂ droplet via the multiphase reaction of SO₂ with NO₂. The sulfate
283 formation was observed only during the multiphase oxidation by NO₂, that is, after the complete conversion of
284 CaCO₃ to Ca(NO₃)₂ droplet. The precipitation of CaSO₄ from solution promoted sulfate formation. The reactive
285 uptake coefficient of SO₂ for sulfate formation in the multiphase reaction with NO₂ is on the order of 10⁻⁸ under
286 the experimental conditions of this study (RH: 46-72%, NO₂: 75 ppm). The reactive uptake coefficient of SO₂
287 was found to be enhanced at higher RH.

288 In order to assess the importance of the multiphase reaction of SO₂ directly oxidized by NO₂ to sulfate in the
289 atmosphere, we compare the lifetime of SO₂ due to the multiphase oxidation of SO₂ by NO₂ with the lifetime due
290 to the gas phase oxidation of SO₂ by OH. Using a daytime OH concentration of 1×10⁶ molecule cm⁻³ (Lelieveld
291 et al., 2016; Prinn et al., 2005), the lifetime of SO₂ in the atmosphere due to gas phase OH oxidation is around 12
292 days. The life time of SO₂ due to the multiphase oxidation by NO₂ is around 7000 days using the uptake
293 coefficient of SO₂ from this study (3.22×10⁻⁸) and a typical particle surface area concentration for mineral
294 aerosols in winter in Beijing (6.3×10⁻⁶ cm² cm⁻³) (Huang et al., 2015). Using an annual average particle surface
295 area concentration of PM₁₀ in Beijing (1.4×10⁻⁵ cm² cm⁻³) (Wehner et al., 2008) results in a SO₂ life time of 3300
296 days due to the multiphase oxidation by NO₂. In the atmosphere, the lifetime of SO₂ due to the multiphase
297 oxidation by NO₂ should be even longer than these values because the uptake coefficient of SO₂ used here
298 (3.22×10⁻⁸) is an upper limit of the uptake coefficient of SO₂ in the ambient atmosphere as discussed above. This
299 comparison indicates that the direct multiphase oxidation of SO₂ by NO₂ is not an important sink of SO₂ and
300 source of sulfate compared with the oxidation of SO₂ by OH.

301 In this study, we used the inert N₂ as a carrier gas for the reaction mixture. In the ambient atmosphere, O₂ is
302 abundantly present and previous studies have suggested that O₂ can enhance the reaction of sulfite with NO₂ in
303 bulk aqueous solution (Littlejohn et al., 1993). Therefore, the potential role of O₂ in the reaction of SO₂ with NO₂
304 in aqueous aerosol particles warrants further studies and will be addressed in a companion paper.

305 Despite the less important role in sulfate formation, the multiphase oxidation of SO₂ by NO₂ on CaCO₃
306 particles helps interpreting the findings from field studies. For example, internally mixed CaCO₃ with Ca(NO₃)₂
307 and CaSO₄ particles with varying reacted fractions of CaCO₃ were observed in the field (Hwang and Ro, 2006; Li
308 and Shao, 2009), but how the internally mixed particles are formed is not clear. In this study we showed that
309 CaSO₄ can be formed inside the Ca(NO₃)₂ droplet after the deliquescence of initially produced Ca(NO₃)₂ through
310 the reaction of SO₂ with NO₂. In this way, internally mixed CaCO₃ with Ca(NO₃)₂ and CaSO₄ particles can be
311 formed. Moreover, Hwang and Ro (2006) found that CaSO₄-containing particles were observed to be almost



312 always internally mixed with nitrate. The multiphase reaction process of SO₂ with NO₂ on CaCO₃ particles found
313 this study can also explain this finding.

314

315 **Acknowledgements**

316 This work was supported by Natural Science Foundation Committee of China (41421064, 21190051,
317 40490265) and Ministry of Science and Technology (Grant No. 2002CB410802).

318 **References**

- 319 Al-Abadleh, H. A., Krueger, B. J., Ross, J. L., and Grassian, V. H.: Phase transitions in calcium nitrate thin films, *Chem.*
320 *Commun.*, 2796-2797, 2003.
- 321 Cao, J. J., Lee, S. C., Zhang, X. Y., Chow, J. C., An, Z. S., Ho, K. F., Watson, J. G., Fung, K., Wang, Y. Q., and Shen, Z. X.:
322 Characterization of airborne carbonate over a site near Asian dust source regions during spring 2002 and its climatic and
323 environmental significance, *J. Geophys. Res.-Atmos.*, 110, 10.1029/2004jd005244, 2005.
- 324 Cheng, Y., Zheng, G., Wei, C., Mu, Q., Zheng, B., Wang, Z., Gao, M., Zhang, Q., He, K., Carmichael, G., Pöschl, U., and
325 Su, H.: Reactive nitrogen chemistry in aerosol water as a source of sulfate during haze events in China, *Sci. Adv.*, 2, 2016.
- 326 Chu, B. W., Zhang, X., Liu, Y. C., He, H., Sun, Y., Jiang, J. K., Li, J. H., and Hao, J. M.: Synergetic formation of secondary
327 inorganic and organic aerosol: effect of SO₂ and NH₃ on particle formation and growth, *Atmos. Chem. Phys.*, 16,
328 14219-14230, 10.5194/acp-16-14219-2016, 2016.
- 329 Clifton, C. L., Altstein, N., and Huie, R. E.: Rate-constant for the reaction of NO₂ with sulfur(IV) over the pH range 5.3-13,
330 *Environ. Sci. Technol.*, 22, 586-589, 10.1021/es00170a018, 1988.
- 331 Cui, H. X., Cheng, T. T., Chen, J. M., Xu, Y. F., and Fang, W.: A Simulated Heterogeneous Reaction of SO₂ on the Surface
332 of Hematite at Different Temperatures, *Acta Phys. Chim. Sin.*, 24, 2331-2336, 10.3866/pku.whxb20081231, 2008.
- 333 Drozd, G., Woo, J., Hakkinen, S. A. K., Nenes, A., and McNeill, V. F.: Inorganic salts interact with oxalic acid in submicron
334 particles to form material with low hygroscopicity and volatility, *Atmos. Chem. Phys.*, 14, 5205-5215,
335 10.5194/acp-14-5205-2014, 2014.
- 336 Ellison, T. K., and Eckert, C. A.: The oxidation of aqueous sulfur dioxide. 4. The influence of nitrogen dioxide at low pH, *J.*
337 *Phys. Chem.*, 88, 2335-2339, 10.1021/j150655a030, 1984.
- 338 Finlayson-Pitts, B., and Pitts Jr., J.: *Chemistry of the upper and lower atmosphere: theory, experiments, and applications*,
339 Academic Press San Diego, 969 pp., 1999.
- 340 Fu, X., Wang, S. X., Chang, X., Cai, S. Y., Xing, J., and Hao, J. M.: Modeling analysis of secondary inorganic aerosols over
341 China: pollution characteristics, and meteorological and dust impacts, *Sci. Rep.*, 6, 10.1038/srep35992, 2016.
- 342 Gao, M., Carmichael, G. R., Wang, Y., Ji, D., Liu, Z., and Wang, Z.: Improving simulations of sulfate aerosols during winter
343 haze over Northern China: the impacts of heterogeneous oxidation by NO₂, *Front. Environ. Sci. Eng.*, 10, 16,
344 10.1007/s11783-016-0878-2, 2016.
- 345 Good, R. J., and Koo, M. N.: Effect of drop size on contact-angle, *J. Colloid Interface Sci.*, 71, 283-292, 1979.
- 346 Goodman, A. L., Li, P., Usher, C. R., and Grassian, V. H.: Heterogeneous uptake of sulfur dioxide on aluminum and
347 magnesium oxide particles, *J. Phys. Chem. A* 105, 6109-6120, 2001.
- 348 Guo, S., Hu, M., Zamora, M. L., Peng, J., Shang, D., Zheng, J., Du, Z., Wu, Z., Shao, M., Zeng, L., Molina, M. J., and Zhang,
349 R.: Elucidating severe urban haze formation in China, *Proc. Nat. Acad. Sci. U.S.A.*, 111, 17373-17378,
350 10.1073/pnas.1419604111, 2014.
- 351 He, H., Wang, Y., Ma, Q., Ma, J., Chu, B., Ji, D., Tang, G., Liu, C., Zhang, H., and Hao, J.: Mineral dust and NO_x promote
352 the conversion of SO₂ to sulfate in heavy pollution days, *Sci. Rep.*, 4, 10.1038/srep04172, 2014.
- 353 Huang, L., Zhao, Y., Li, H., and Chen, Z.: Kinetics of Heterogeneous Reaction of Sulfur Dioxide on Authentic Mineral Dust:
354 Effects of Relative Humidity and Hydrogen Peroxide, *Environ. Sci. Technol.*, 49, 10797-10805, 10.1021/acs.est.5b03930,
355 2015.
- 356 Huang, L. B., Zhao, Y., Li, H., and Chen, Z. M.: Hydrogen peroxide maintains the heterogeneous reaction of sulfur dioxide
357 on mineral dust proxy particles, *Atmos. Environ.*, 141, 552-559, 10.1016/j.atmosenv.2016.07.035, 2016.
- 358 Huang, X., Song, Y., Zhao, C., Li, M., Zhu, T., Zhang, Q., and Zhang, X.: Pathways of sulfate enhancement by natural and
359 anthropogenic mineral aerosols in China, *J. Geophys. Res.-Atmos.*, 119, 14,165-114,179, 10.1002/2014jd022301, 2014.



- 360 Hwang, H. J., and Ro, C. U.: Direct observation of nitrate and sulfate formations from mineral dust and sea-salts using low-Z
361 particle electron probe X-ray microanalysis, *Atmos. Environ.*, 40, 3869-3880, 10.1016/j.atmosenv.2006.02.022, 2006.
- 362 Kong, L. D., Zhao, X., Sun, Z. Y., Yang, Y. W., Fu, H. B., Zhang, S. C., Cheng, T. T., Yang, X., Wang, L., and Chen, J. M.:
363 The effects of nitrate on the heterogeneous uptake of sulfur dioxide on hematite, *Atmos. Chem. Phys.*, 14, 9451-9467,
364 10.5194/acp-14-9451-2014, 2014.
- 365 Krueger, B. J., Grassian, V. H., Cowin, J. P., and Laskin, A.: Heterogeneous chemistry of individual mineral dust particles
366 from different dust source regions: the importance of particle mineralogy, *Atmos. Environ.*, 38, 6253-6261,
367 10.1016/j.atmosenv.2004.07.010, 2004.
- 368 Laskin, A., Iedema, M. J., Ichkovich, A., Graber, E. R., Taraniuk, I., and Rudich, Y.: Direct observation of completely
369 processed calcium carbonate dust particles, *Faraday Discuss.*, 130, 453-468, 10.1039/b417366j, 2005.
- 370 Lee, Y.-N., and Schwartz, S. E.: Kinetics of oxidation of aqueous sulfur (IV) by nitrogen dioxide, in: *Precipitation*
371 *Scavenging, Dry Deposition and Resuspension*, edited by: Pruppacher, H. R., Semonin, R. G., and Slinn, W. G. N., Elsevier,
372 New York, 453-466, 1983.
- 373 Lelieveld, J., Gromov, S., Pozzer, A., and Taraborrelli, D.: Global tropospheric hydroxyl distribution, budget and reactivity,
374 *Atmos. Chem. Phys.*, 16, 12477-12493, 10.5194/acp-16-12477-2016, 2016.
- 375 Li, H. J., Zhu, T., Zhao, D. F., Zhang, Z. F., and Chen, Z. M.: Kinetics and mechanisms of heterogeneous reaction of NO₂
376 on CaCO₃ surfaces under dry and wet conditions, *Atmos. Chem. Phys.*, 10, 463-474, 2010.
- 377 Li, J., Shang, J., and Zhu, T.: Heterogeneous reactions of SO₂ on ZnO particle surfaces, *Sci. China Chem.*, 54, 161-166,
378 10.1007/s11426-010-4167-9, 2011.
- 379 Li, L., Chen, Z. M., Ding, J., Zhu, T., and Zhang, Y. H.: A DRIFTS study of SO₂ oxidation on the surface of CaCO₃
380 particles, *Spectrosc. Spect. Anal.*, 24, 1556-1559, 2004.
- 381 Li, L., Chen, Z. M., Zhang, Y. H., Zhu, T., Li, J. L., and Ding, J.: Kinetics and mechanism of heterogeneous oxidation of
382 sulfur dioxide by ozone on surface of calcium carbonate, *Atmos. Chem. Phys.*, 6, 2453-2464, 2006.
- 383 Li, L., Chen, Z. M., Zhang, Y. H., Zhu, T., Li, S., Li, H. J., Zhu, L. H., and Xu, B. Y.: Heterogeneous oxidation of sulfur
384 dioxide by ozone on the surface of sodium chloride and its mixtures with other components, *J. Geophys. Res.-Atmos.*, 112,
385 10.1029/2006jd008207, 2007.
- 386 Li, W. J., and Shao, L. Y.: Observation of nitrate coatings on atmospheric mineral dust particles, *Atmos. Chem. Phys.*, 9,
387 1863-1871, 2009.
- 388 Lide, D. R.: *CRC Handbook of Chemistry and Physics*, 89 ed., CRC Press/Taylor and Francis, Boca Raton, FL, 2009.
- 389 Littlejohn, D., Wang, Y. Z., and Chang, S. G.: Oxidation of aqueous sulfite ion by nitrogen-dioxide, *Environ. Sci. Technol.*,
390 27, 2162-2167, 10.1021/es00047a024, 1993.
- 391 Liu, C., Ma, Q. X., Liu, Y. C., Ma, J. Z., and He, H.: Synergistic reaction between SO₂ and NO₂ on mineral oxides: a
392 potential formation pathway of sulfate aerosol, *Phys. Chem. Chem. Phys.*, 14, 1668-1676, 10.1039/c1cp22217a, 2012.
- 393 Liu, Y. J., Zhu, T., Zhao, D. F., and Zhang, Z. F.: Investigation of the hygroscopic properties of Ca(NO₃)₂ and internally
394 mixed Ca(NO₃)₂/CaCO₃ particles by micro-Raman spectrometry, *Atmos. Chem. Phys.*, 8, 7205-7215, 2008.
- 395 Ma, Q., He, H., Liu, Y., Liu, C., and Grassian, V. H.: Heterogeneous and multiphase formation pathways of gypsum in the
396 atmosphere, *Phys. Chem. Chem. Phys.*, 15, 19196-19204, 10.1039/c3cp53424c, 2013a.
- 397 Ma, Q., Wang, T., Liu, C., He, H., Wang, Z., Wang, W., and Liang, Y.: SO₂ Initiates the Efficient Conversion of NO₂ to
398 HONO on MgO Surface, *Environ. Sci. Technol.*, 51, 3767-3775, 10.1021/acs.est.6b05724, 2017.
- 399 Ma, Q. X., Liu, Y. C., and He, H.: Synergistic effect between NO₂ and SO₂ in their adsorption and reaction on
400 gamma-alumina, *J. Phys. Chem. A* 112, 6630-6635, 10.1021/jp802025z, 2008.
- 401 Ma, Q. X., and He, H.: Synergistic effect in the humidifying process of atmospheric relevant calcium nitrate, calcite and
402 oxalic acid mixtures, *Atmos. Environ.*, 50, 97-102, 10.1016/j.atmosenv.2011.12.057, 2012.



- 403 Ma, Q. X., He, H., Liu, Y. C., Liu, C., and Grassian, V. H.: Heterogeneous and multiphase formation pathways of gypsum in
404 the atmosphere, *Phys. Chem. Chem. Phys.*, 15, 19196-19204, 10.1039/c3cp53424c, 2013b.
- 405 Martin, L. R., Damschen, D. E., and Judeikis, H. S.: The reactions of nitrogen-oxides with SO₂ in aqueous aerosols, *Atmos.*
406 *Environ.*, 15, 191-195, 10.1016/0004-6981(81)90010-x, 1981.
- 407 Nakamoto, K.: *Infrared and Raman Spectra of Inorganic and Coordination Compounds*, John Wiley & Sons, New York,
408 1997.
- 409 Okada, K., Qin, Y., and Kai, K.: Elemental composition and mixing properties of atmospheric mineral particles collected in
410 Hohhot, China, *Atmos. Res.*, 73, 45-67, 2005.
- 411 Park, J. Y., and Jang, M.: Heterogeneous photooxidation of sulfur dioxide in the presence of airborne mineral dust particles,
412 *Rsc Advances*, 6, 58617-58627, 10.1039/c6ra09601h, 2016.
- 413 Passananti, M., Kong, L. D., Shang, J., Dupart, Y., Perrier, S., Chen, J. M., Donaldson, D. J., and George, C.: Organosulfate
414 Formation through the Heterogeneous Reaction of Sulfur Dioxide with Unsaturated Fatty Acids and Long-Chain Alkenes,
415 *Angew. Chem.-Int. Edit.*, 55, 10336-10339, 10.1002/anie.201605266, 2016.
- 416 Prince, A. P., Grassian, V. H., Kleiber, P., and Young, M. A.: Heterogeneous conversion of calcite aerosol by nitric acid,
417 *Phys. Chem. Chem. Phys.*, 9, 622-634, 2007a.
- 418 Prince, A. P., Kleiber, P., Grassian, V. H., and Young, M. A.: Heterogeneous interactions of calcite aerosol with sulfur
419 dioxide and sulfur dioxide-nitric acid mixtures, *Phys. Chem. Chem. Phys.*, 9, 3432-3439, 2007b.
- 420 Prinn, R. G., Huang, J., Weiss, R. F., Cunnold, D. M., Fraser, P. J., Simmonds, P. G., McCulloch, A., Harth, C., Reimann, S.,
421 Salameh, P., O'Doherty, S., Wang, R. H. J., Porter, L. W., Miller, B. R., and Krummel, P. B.: Evidence for variability of
422 atmospheric hydroxyl radicals over the past quarter century, *Geophys. Res. Lett.*, 32, 10.1029/2004gl022228, 2005.
- 423 Rosenberg, H. S., and Grotta, H. M.: Nitrogen oxides (NO_x) influence on sulfite oxidation and scaling in lime/limestone flue
424 gas desulfurization (FGD) systems, *Environ. Sci. Technol.*, 14, 470-472, 10.1021/es60164a011, 1980.
- 425 Sarma, L. P., Prasad, P. S. R., and Ravikumar, N.: Raman spectroscopic study of phase transitions in natural gypsum, *J.*
426 *Raman Spectrosc.*, 29, 851-856, 10.1002/(sici)1097-4555(199809)29:9<851::aid-jrs313>3.0.co;2-s, 1998.
- 427 Seinfeld, J. H., and Pandis, S. N.: *Atmospheric chemistry and physics: from air pollution to climate change*, 2nd ed., John
428 Wiley & Sons, Inc., 2006.
- 429 Shang, J., Li, J., and Zhu, T.: Heterogeneous reaction of SO₂ on TiO₂ particles, *Sci. China Chem.*, 53, 2637-2643,
430 10.1007/s11426-010-4160-3, 2010.
- 431 Shen, C. H., and Rochelle, G. T.: Nitrogen Dioxide Absorption and Sulfite Oxidation in Aqueous Sulfite, *Environ. Sci.*
432 *Technol.*, 32, 1994-2003, 10.1021/es970466q, 1998.
- 433 Song, C. H., Maxwell-Meier, K., Weber, R. J., Kapustin, V., and Clarke, A.: Dust composition and mixing state inferred
434 from airborne composition measurements during ACE-Asia C130 Flight #6, *Atmos. Environ.*, 39, 359-369, 2005.
- 435 Sorimachi, A., Sakai, M., Ishitani, O., Nishikawa, M., and Sakamoto, K.: Study on dry deposition of SO₂-NO_x onto loess,
436 *Water Air Soil Pollut.*, 130, 541-546, 10.1023/a:1013834729728, 2001.
- 437 Tang, I. N., and Fung, K. H.: Hydration and Raman scattering studies of levitated microparticles: Ba(NO₃)₂, Sr(NO₃)₂,
438 and Ca(NO₃)₂, *J. Chem. Phys.*, 106, 1653-1660, 1997.
- 439 Tobo, Y., Zhang, D. Z., Matsuki, A., and Iwasaka, Y.: Asian dust particles converted into aqueous droplets under remote
440 marine atmospheric conditions, *Proc. Nat. Acad. Sci. U.S.A.*, 107, 17905-17910, 10.1073/pnas.1008235107, 2010.
- 441 Ullerstam, M., Vogt, R., Langer, S., and Ljungstrom, E.: The kinetics and mechanism of SO₂ oxidation by O₃ on mineral
442 dust, *Phys. Chem. Chem. Phys.*, 4, 4694-4699, 10.1039/b203529b, 2002.
- 443 Ullerstam, M., Johnson, M. S., Vogt, R., and Ljungstrom, E.: DRIFTS and Knudsen cell study of the heterogeneous
444 reactivity of SO₂ and NO₂ on mineral dust, *Atmos. Chem. Phys.*, 3, 2043-2051, 2003.



- 445 Wang, G., Zhang, R., Gomez, M. E., Yang, L., Levy Zamora, M., Hu, M., Lin, Y., Peng, J., Guo, S., Meng, J., Li, J., Cheng,
446 C., Hu, T., Ren, Y., Wang, Y., Gao, J., Cao, J., An, Z., Zhou, W., Li, G., Wang, J., Tian, P., Marrero-Ortiz, W., Secretst, J.,
447 Du, Z., Zheng, J., Shang, D., Zeng, L., Shao, M., Wang, W., Huang, Y., Wang, Y., Zhu, Y., Li, Y., Hu, J., Pan, B., Cai, L.,
448 Cheng, Y., Ji, Y., Zhang, F., Rosenfeld, D., Liss, P. S., Duce, R. A., Kolb, C. E., and Molina, M. J.: Persistent sulfate
449 formation from London Fog to Chinese haze, *Proc. Nat. Acad. Sci. U.S.A.*, 113, 13630-13635, 10.1073/pnas.1616540113,
450 2016.
- 451 Wang, Y. S., Yao, L., Wang, L. L., Liu, Z. R., Ji, D. S., Tang, G. Q., Zhang, J. K., Sun, Y., Hu, B., and Xin, J. Y.:
452 Mechanism for the formation of the January 2013 heavy haze pollution episode over central and eastern China, *Sci. China*
453 *Earth Sci.*, 57, 14-25, 10.1007/s11430-013-4773-4, 2014a.
- 454 Wang, Y. X., Zhang, Q. Q., Jiang, J. K., Zhou, W., Wang, B. Y., He, K. B., Duan, F. K., Zhang, Q., Philip, S., and Xie, Y.
455 Y.: Enhanced sulfate formation during China's severe winter haze episode in January 2013 missing from current models, *J.*
456 *Geophys. Res.-Atmos.*, 119, 10.1002/2013jd021426, 2014b.
- 457 Wehner, B., Birmili, W., Ditas, F., Wu, Z., Hu, M., Liu, X., Mao, J., Sugimoto, N., and Wiedensohler, A.: Relationships
458 between submicrometer particulate air pollution and air mass history in Beijing, China, 2004–2006, *Atmos. Chem. Phys.*, 8,
459 6155-6168, 10.5194/acp-8-6155-2008, 2008.
- 460 Wu, L. Y., Tong, S. R., Wang, W. G., and Ge, M. F.: Effects of temperature on the heterogeneous oxidation of sulfur dioxide
461 by ozone on calcium carbonate, *Atmos. Chem. Phys.*, 11, 6593-6605, 10.5194/acp-11-6593-2011, 2011.
- 462 Wu, L. Y., Tong, S. R., Zhou, L., Wang, W. G., and Ge, M. F.: Synergistic Effects between SO₂ and HCOOH on
463 alpha-Fe₂O₃, *J. Phys. Chem. A* 117, 3972-3979, 10.1021/jp400195f, 2013.
- 464 Wu, L. Y., Tong, S. R., and Ge, M. F.: Synergistic Effect between SO₂ and HCOOH on the Surface of CaO, *Acta Chim.*
465 *Sinica* 73, 131-136, 10.6023/a14120875, 2015.
- 466 Xie, Y. N., Ding, A. J., Nie, W., Mao, H. T., Qi, X. M., Huang, X., Xu, Z., Kerminen, V. M., Petaja, T., Chi, X. G., Virkkula,
467 A., Boy, M., Xue, L. K., Guo, J., Sun, J. N., Yang, X. Q., Kulmala, M., and Fu, C. B.: Enhanced sulfate formation by
468 nitrogen dioxide: Implications from in situ observations at the SORPES station, *J. Geophys. Res.-Atmos.*, 120, 12679-12694,
469 10.1002/2015jd023607, 2015.
- 470 Xue, J., Yuan, Z. B., Griffith, S. M., Yu, X., Lau, A. K. H., and Yu, J. Z.: Sulfate Formation Enhanced by a Cocktail of High
471 NO_x, SO₂, Particulate Matter, and Droplet pH during Haze-Fog Events in Megacities in China: An Observation-Based
472 Modeling Investigation, *Environ. Sci. Technol.*, 50, 7325-7334, 10.1021/acs.est.6b00768, 2016.
- 473 Zhang, D. Z., Shi, G. Y., Iwasaka, Y., and Hu, M.: Mixture of sulfate and nitrate in coastal atmospheric aerosols: individual
474 particle studies in Qingdao (36 degrees 04 ' N, 120 degrees 21 ' E), China, *Atmos. Environ.*, 34, 2669-2679,
475 10.1016/s1352-2310(00)00078-9, 2000.
- 476 Zhang, J. K., Sun, Y., Liu, Z. R., Ji, D. S., Hu, B., Liu, Q., and Wang, Y. S.: Characterization of submicron aerosols during a
477 month of serious pollution in Beijing, 2013, *Atmos. Chem. Phys.*, 14, 2887-2903, 10.5194/acp-14-2887-2014, 2014.
- 478 Zhang, Q., Jimenez, J. L., Canagaratna, M. R., Allan, J. D., Coe, H., Ulbrich, I., Alfarra, M. R., Takami, A., Middlebrook, A.
479 M., Sun, Y. L., Dzepina, K., Dunlea, E., Docherty, K., DeCarlo, P. F., Salcedo, D., Onasch, T., Jayne, J. T., Miyoshi, T.,
480 Shimono, A., Hatakeyama, S., Takegawa, N., Kondo, Y., Schneider, J., Drewnick, F., Borrmann, S., Weimer, S., Demerjian,
481 K., Williams, P., Bower, K., Bahreini, R., Cottrell, L., Griffin, R. J., Rautiainen, J., Sun, J. Y., Zhang, Y. M., and Worsnop,
482 D. R.: Ubiquity and dominance of oxygenated species in organic aerosols in anthropogenically-influenced Northern
483 Hemisphere midlatitudes, *Geophys. Res. Lett.*, 34, 10.1029/2007gl029979, 2007.
- 484 Zhao, D. F., Zhu, T., Chen, Q., Liu, Y. J., and Zhang, Z. F.: Raman micro-spectrometry as a technique for investigating
485 heterogeneous reactions on individual atmospheric particles, *Sci. China Chem.*, 54, 154-160, 10.1007/s11426-010-4182-x,
486 2011.



487 Zhao, X., Kong, L. D., Sun, Z. Y., Ding, X. X., Cheng, T. T., Yang, X., and Chen, J. M.: Interactions between
488 Heterogeneous Uptake and Adsorption of Sulfur Dioxide and Acetaldehyde on Hematite, *J. Phys. Chem. A* 119, 4001-4008,
489 10.1021/acs.jpca.5b01359, 2015.

490 Zheng, B., Zhang, Q., Zhang, Y., He, K. B., Wang, K., Zheng, G. J., Duan, F. K., Ma, Y. L., and Kimoto, T.: Heterogeneous
491 chemistry: a mechanism missing in current models to explain secondary inorganic aerosol formation during the January 2013
492 haze episode in North China, *Atmos. Chem. Phys.*, 15, 2031-2049, 10.5194/acp-15-2031-2015, 2015a.

493 Zheng, G. J., Duan, F. K., Su, H., Ma, Y. L., Cheng, Y., Zheng, B., Zhang, Q., Huang, T., Kimoto, T., Chang, D., Poschl, U.,
494 Cheng, Y. F., and He, K. B.: Exploring the severe winter haze in Beijing: the impact of synoptic weather, regional transport
495 and heterogeneous reactions, *Atmos. Chem. Phys.*, 15, 2969-2983, 10.5194/acp-15-2969-2015, 2015b.

496 Zhou, L., Wang, W. G., Gai, Y. B., and Ge, M. F.: Knudsen cell and smog chamber study of the heterogeneous uptake of
497 sulfur dioxide on Chinese mineral dust, *J. Environ. Sci.*, 26, 2423-2433, 10.1016/j.jes.2014.04.005, 2014.

498 Zhu, T., Shang, J., and Zhao, D. F.: The roles of heterogeneous chemical processes in the formation of an air pollution
499 complex and gray haze, *Sci. China Chem.*, 54, 145-153, 10.1007/s11426-010-4181-y, 2011.

500



502 Table 1 Summary of the results obtained in different reaction systems

Particle	Gases	RH (%)	Whether sulfate was detected
CaCO ₃	SO ₂ (75 ppm)+NO ₂ (75 ppm)	72	Yes
Ca(NO ₃) ₂ droplet	SO ₂ (75 ppm)+NO ₂ (75 ppm)	72	Yes
CaCO ₃	SO ₂ (150 ppm)	72	No
Ca(NO ₃) ₂ droplet	SO ₂ (150 ppm))	72	No
NaNO ₃ droplet	SO ₂ (75 ppm)+NO ₂ (75 ppm)	72	No
NH ₄ NO ₃ droplet	SO ₂ (75 ppm)+NO ₂ (75 ppm)	72	No

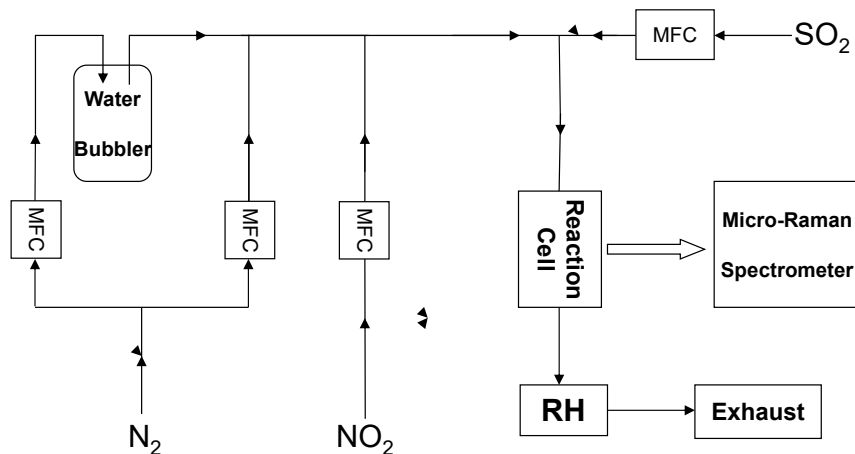
503



504 Table 2. Reactive uptake coefficient of SO₂ for sulfate formation (γ) during the reaction of SO₂ with NO₂ on
505 individual CaCO₃ particles under different conditions at 298 K.

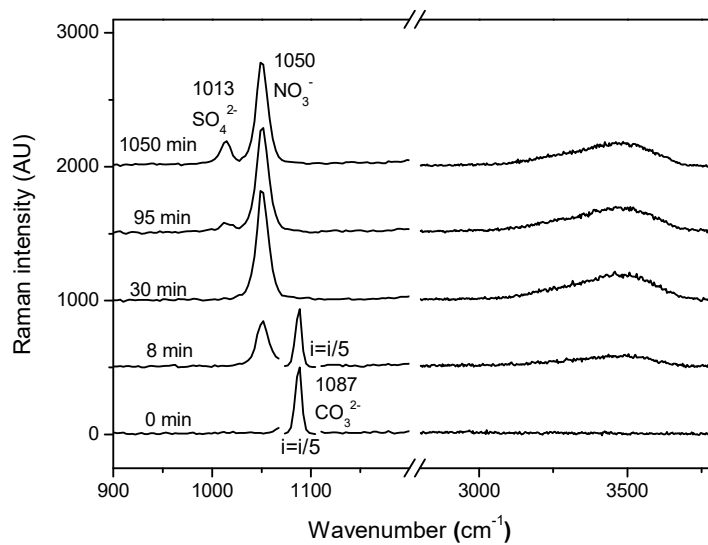
[SO ₂] (ppm)	[NO ₂] (ppm)	RH (%)	γ ($\times 10^{-8}$)
75	75	72	3.22±1.08
75	200	72	16.0±3.12
75	75	46	3.22±0.90
75	75	17	0 ^a
200	200	17	0 ^a

506 ^a: Sulfate was below the detection limit.



507

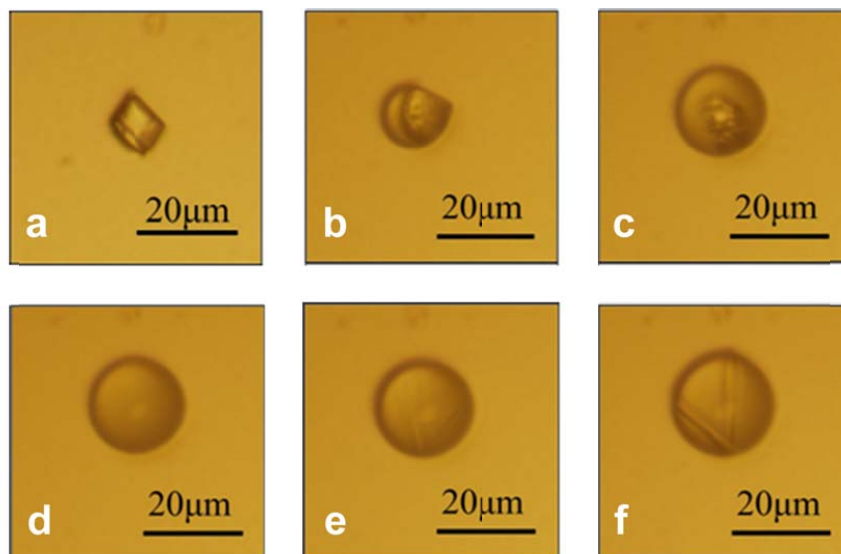
508 Fig. 1. Schematic diagram of the experimental setup. MFC: mass flow controller.



509

510 Fig. 2. Raman spectra of an individual CaCO₃ particle during the reaction with NO₂ (75 ppm) and SO₂ (75 ppm)

511 at 72% RH at the reaction time of 0, 8, 30, 95, and 1050 min.

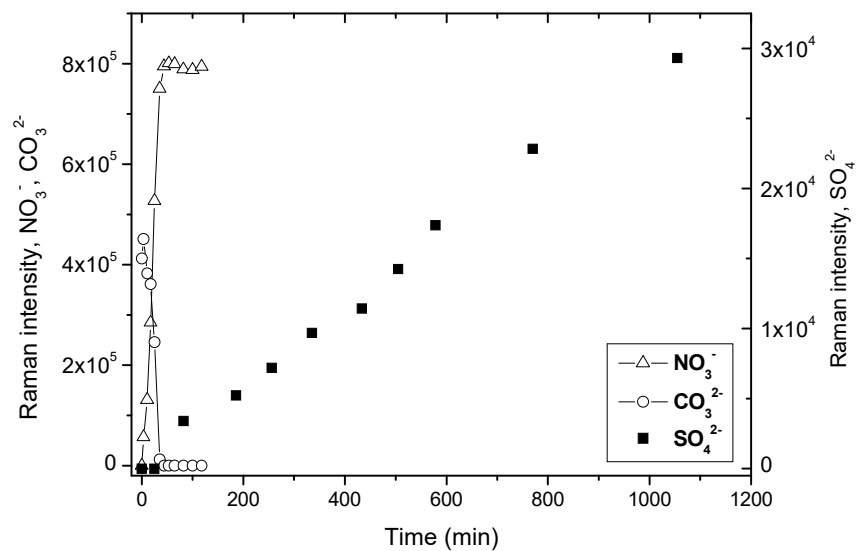


512

513 Fig. 3. Microscopic images of an individual CaCO_3 particle (same as in Fig. 2) reacting with NO_2 (75 ppm) and

514 SO_2 (75 ppm) at 72% RH. a-f corresponds to the reaction time of 0, 6, 29, 37, 94, and 1050 min, respectively.

515



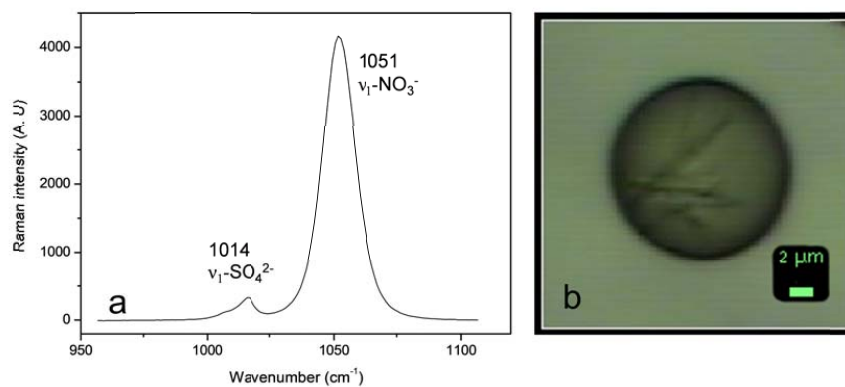
516

517 Fig. 4. Raman peak intensity of carbonate, nitrate (left axis), and sulfate (right axis) as a function of time during
518 the reaction of an individual CaCO₃ particle with NO₂ (75ppm) and SO₂ (75ppm) at 72% RH (same as in Fig. 2
519 and 3). Note that the scales of the left axis and right axis are different. The intensity of NO₃⁻, SO₄²⁻, and CO₃²⁻
520 show the peak area at 1050, 1013, and 1087 cm⁻¹, respectively, in Raman spectra obtained by Raman mapping.

521



522

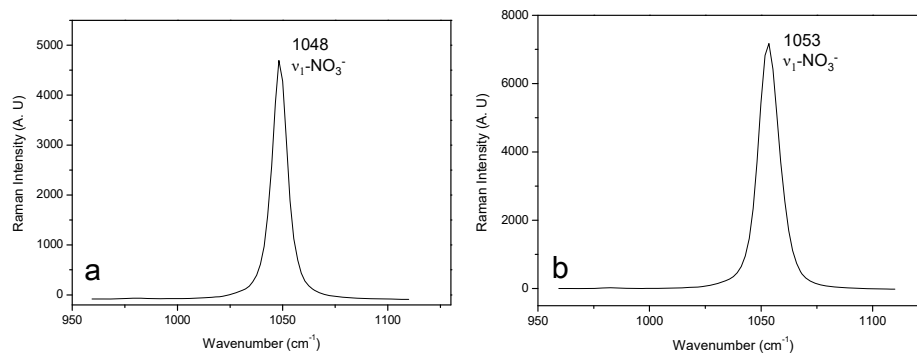


523

524 Fig. 5. Raman spectra (a) and microscopic image (b) of a $\text{Ca}(\text{NO}_3)_2$ droplet reacting with NO_2 (75 ppm) and SO_2
525 (75 ppm) at 72% RH at a reaction time of 300 min. The peak at 1014 cm^{-1} in Raman spectra and crystals from the
526 microscopic image indicate CaSO_4 was formed in this reaction.



527



528

529 Fig. 6. Raman spectra of a NH_4NO_3 (a) and NaNO_3 (b) droplet reacting with NO_2 (75 ppm) and SO_2 (75 ppm) at

530 72% RH at the reaction time of 300 min.

531